

# Specific Capacitance Dependence on the Specific Resistance in Nb/Al-AlO<sub>x</sub>/Nb Tunnel Junctions

Parisa Yadranjee Aghdam, Hawal Rashid, Alexey Pavolotsky, Vincent Desmaris, Denis Meledin, Victor Belitsky

**Abstract**— The junction specific capacitance ( $C_s$ ) is an essential parameter in designing tuning circuitry for Superconductor-Insulator-Superconductor (SIS) mixers. However, our knowledge of the junction capacitance only relies on the few available empirically obtained  $C_s$  vs. specific normal resistance ( $R_nA$ ) relations, which are inconsistent especially at low  $R_nA$  values,  $R_nA < 40 \Omega \cdot \mu\text{m}^2$ . In this paper, we report the Nb/Al-AlO<sub>x</sub>/Nb SIS junction capacitance data from our recently presented direct microwave (4 GHz) measurements at 4K for junctions with various  $R_nA$  values ranging from 8.8 to 68  $\Omega \cdot \mu\text{m}^2$ . New insight is provided into the extraction of the true geometrical specific capacitance of SIS junctions. We show that, even at such low microwave frequencies, the so-far-neglected nonlinear susceptance is significant, especially for junctions with low  $R_nA$  values. This susceptance originates from the real part of the response function,  $I_{KK}$ , which can be calculated through the Kramers-Kronig transform of the DC tunnel current. The new specific capacitance, which accounts for this contribution is presented as a function of  $R_nA$ . We provide an improved and more accurate  $C_s$  ( $R_nA$ ) relation, which can be a reliable and useful tool for circuit designers. The obtained  $C_s$  ( $R_nA$ ) relation is compared with those available in the literature, and the possible reasons giving rise to the disparity among these relations are discussed. By comparing the modelled and the measured noise temperature of the APEX SHeFI band 3 (385–500 GHz) DSB mixer, we show that the new  $C_s$  ( $R_nA$ ) relation offers a great potential for improving the performance of SIS mixers.

**Index Terms**—Capacitance measurement, Microwave measurement, Superconducting microwave devices, Tunnel junctions, Submillimeter wave devices, superconductor-insulator-superconductor (SIS) mixer

## I. INTRODUCTION

Superconductor-Insulator-Superconductor (SIS) mixers have become the cornerstone of most low noise heterodyne receivers for radio astronomical spectroscopy in millimeter and submillimeter range [5]. In the last few years there has been a growing interest in improving capabilities of radio astronomical receivers in terms of wider instantaneous RF and IF bandwidth [6]–[8]. One of the advantages of a wide RF instantaneous bandwidth is to reduce the number of instruments for conducting observations. A wide IF bandwidth, on the other hand, provides simultaneous detection of several spectral lines

or more effective line surveys.

The instantaneous IF bandwidth is partly limited by the relatively high capacitance of SIS junctions. For an SIS mixer to have a wide RF bandwidth, a low  $\omega RC$  product (where  $R$  and  $C$  are the junction resistance and capacitance, respectively), and as it is shown in [4] a low specific normal resistance ( $R_nA$ ) ( $R_nA < 20 \Omega \cdot \mu\text{m}^2$ ) are needed. For both cases, the junction specific capacitance ( $C_s$ ) plays a crucial role in designing tuning circuitry for SIS mixers [9]. Moreover, the precise knowledge of junction specific capacitance is also needed in other applications of SIS tunnel junctions such as qubits [10], [11], single charge [12], [13] and digital devices [1], [14], where  $C_s$  determines other junction characteristics such as the RC time constant, the charging energy and the so called plasma frequency.

The literature on the specific capacitance of Nb/Al-AlO<sub>x</sub>/Nb SIS junction shows a few measurement approaches in which the junction capacitance is measured for single values or different ranges of  $R_nA$  [1]–[3], [15]–[17]. All of these approaches, except for our recently presented method in [17], employed indirect measurement methods, in which the capacitive effect of the SIS junction, e.g., resonance or dispersion of the resonant frequencies is measured. In these studies, models were fitted to the experimentally obtained  $C_s$  ( $R_nA$ ) relation (see Figure 1). As can be seen from this figure, the  $C_s$  ( $R_nA$ ) relations significantly

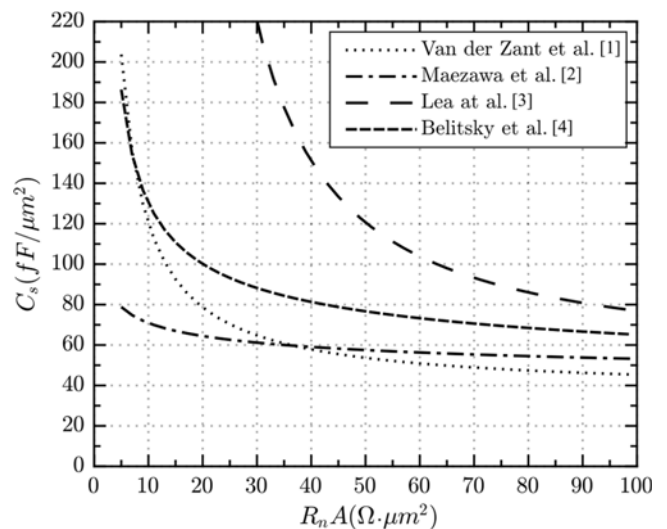


Fig. 1. The existing empirically [1]–[3] and semi-empirically [4] models for the  $C_s$  vs.  $R_nA$  relation of Nb/Al-AlO<sub>x</sub>/Nb SIS junction.

diverge from each other for  $R_n A < 40 \Omega \cdot \mu\text{m}^2$  [1]–[4]. The measured  $R_n A$  range in these models were as follows:  $R_n A \approx 10\text{--}2000 \Omega \cdot \mu\text{m}^2$  [2],  $R_n A \approx 10\text{--}1000 \Omega \cdot \mu\text{m}^2$  [1],  $R_n A \approx 40\text{--}4000 \Omega \cdot \mu\text{m}^2$  [3].

On the one hand, it can be hypothesized that the different measurement methods of the junction capacitance and their related measurement uncertainties could be the reason for the observed disparity. In this regard, not only the uncertainty of the capacitance estimation depends on the accuracy of the measurements themselves, but also on the assumptions made in the often very complex employed models as well as the used material parameters. On the other hand, as we reported previously in [18], the observed scatter in the measurements of the  $R_n C$  for the same  $R_n A$  value could likely be due to the local non-uniformities in the tunnel barrier thickness, which then result in the scatter of both  $C_s$  and  $R_n A$ .

In this paper, we use the measurement results for Nb/Al-AIO<sub>x</sub>/Nb SIS junction capacitance, based on direct microwave measurements [17], for  $R_n A$  range of 8.8–68  $\Omega \cdot \mu\text{m}^2$ . The employed method offers direct junction capacitance measurements with high accuracy at microwave frequencies [17]. In Subsection A, we discuss the extraction of the true geometrical junction capacitance. In this context, we underline that even at such low frequencies, the susceptance, which is obtained by the Kramers-Kronig transformation of the imaginary part of the response function (i.e. quasiparticle dc IV characteristics), should be calculated and subtracted from the measured capacitance. Also, we show that this susceptance, which is capacitive under the conducted measurement conditions and hereafter will be referred to as the nonlinear capacitance, is non-negligible for junctions with low  $R_n A$  values. We argue that neglecting such contributions might have resulted in over estimation of junction capacitance in certain capacitance measurement methods. However, as will be discussed in the present paper, the scatter resulted from neglecting the nonlinear susceptance, and the effect of local non-uniformities in the tunnel barrier still cannot explain some cases of the observed disparity in Figure 1. This indicates that the main reason giving rise to the divergent  $C_s$  ( $R_n A$ ) relations is the difference in the nature of the measurement methods and their related uncertainty. In addition, some specifics of the junction fabrication process could possibly contribute to the observed differences. Employing the direct method in this study and obtaining the true geometrical specific capacitance, an improved and more accurate  $C_s$  ( $R_n A$ ) relation is obtained, which can be a reliable and useful tool for circuit designers. The potential for an improved performance of the SIS mixer by using the suggested  $C_s$  ( $R_n A$ ) relation is shown by comparing the modelled and measured noise temperature for the band 3 (385–500 GHz) DSB mixer in Atacama Pathfinder Experiment (APEX) telescope.

## II. EXPERIMENTAL

A total of 34 Nb/Al-AIO<sub>x</sub>/Nb SIS junctions with  $R_n A$  range of

8.8–68  $\Omega \cdot \mu\text{m}^2$  were fabricated. The details of the trilayer deposition parameters and the junction fabrication process were presented in [17], [19]. The AlO<sub>x</sub> oxygen exposure parameters for the 34 junctions are presented in details in our recent publication [18] and are listed in Table I. The junctions' nominal areas on the used photomask were:  $A_1=3.6 \mu\text{m}^2$ ,  $A_2=4.4 \mu\text{m}^2$ ,  $A_3=6 \mu\text{m}^2$ ,  $A_4=10.8 \mu\text{m}^2$  and  $A_5=20 \mu\text{m}^2$ . For each processed wafer, the true junction sizes ( $A$ ) were estimated [17], which accounted for the dimension variation due to the fabrication process (lithography and etch process). The junction normal resistance  $R_n$ , was extracted from the IV characteristic recorded in liquid helium [18]. The product of the extracted  $R_n$  and the estimated area,  $A$ , which is the junction specific resistance ( $R_n A$ ), were used as the measure of the tunnel barrier transparency. The fabricated junctions in the abovementioned  $R_n A$  range were all of high quality with the superconducting gap voltage variation of  $V_g \approx 2.84\text{--}2.88$  mV and the junction quality factor of subgap resistance ( $R_{sg}$ )/ $R_n \approx 17\text{--}44$  [18]. The complex impedance of these junctions were directly measured at 4 GHz center frequency and at 4 K temperature. The calibration at 4 K was performed using the time-domain processing techniques and the gap voltage biased junction as the short-circuit reference [20]. Then an Agilent ADS equivalent circuit model [17] was used in which the model parameters were adjusted based on the calibration. Later the SIS junction capacitance was extracted once the best fit was achieved between the model and the experimental data. More details on this procedure can be found in [17].

TABLE I  
OXYGEN EXPOSURE ( $E$ ) OF THE USED SIX BATCHES. THE NUMBER OF CHARACTERIZED CHIPS IS INDICATED. DATA FROM [18]

Batch #	1	2	3	4	5	6
$E$ (Pas)	1530	1530	2500	2500	6200	13000
Wafers	1	1	1	1	2	2
Chips	3	5	5	5	8	8

## III. RESULTS AND DISCUSSION

### A. The specific capacitance

The measurement results of the extracted junction capacitance ( $C_m$ ) as a function of the estimated area ( $A$ ) for each batch of junctions, are presented as solid grey circles in Figure 2a-f. Assuming the parallel-plate approximation, i.e., linear dependence of the junction capacitance on the junction area, the data is fitted with linear regression lines (dotted lines). The  $C_s$  is then extracted as the slope of these lines (in pF/ $\mu\text{m}^2$ ), which is indicated above each fitted line. The linear fit through the data points in Figure 2 contained non-zero intercepts. However, the observed intercepts were proved to be statistically insignificant. Consequently, the specific capacitance data is presented for the linear regression with intercepts set to zero.

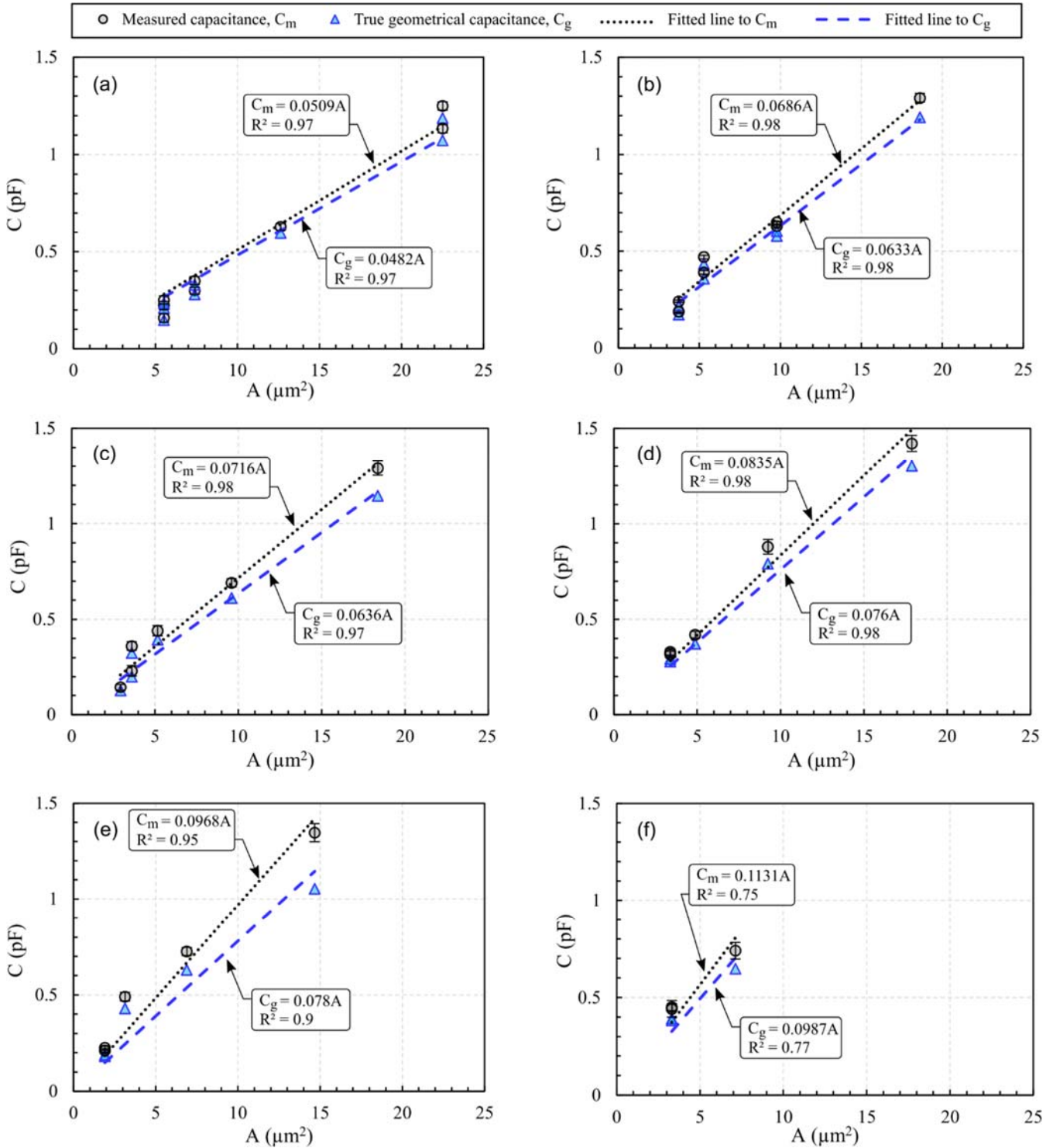


Fig. 2. The measured ( $C_m$ ) and the true geometrical capacitance ( $C_g$ ) as a function of the estimated area ( $A$ ). These results are presented for batches with  $R_n A$  (in  $\Omega \cdot \mu\text{m}^2$ ) values of: (a) 68, (b) 33.8, (c) 23, (d) 19, (e) 9.4, and (f) 8.8. The error bars on the  $C_m$  data points represent the estimated measurement uncertainty [17]. In order to prevent cluttering of the plot, the error bars on  $C_g$  (which are the same as that of the  $C_m$ ) are not shown in the plot. From the slope of the linear fit to the measured and the corrected junction capacitance, the resulting specific capacitance values are obtained.

In order to ensure that the measured capacitance could only be attributed to the geometrical junction capacitance, all the other possible contributions such as stray capacitance, fringing field capacitance, etc., were investigated. It was concluded in [18] that such contributions were negligible. The only significant contribution was found to be from what we call the nonlinear susceptance. Even though, this contribution has always been

neglected when operating at frequencies of a few GHz, our calculations show its significance.

The measurable quasiparticle tunnel current at the dc I-V characteristic of the junction is considered as the dissipative component of the tunnel current. The extreme nonlinearity of this dc I-V relation at the gap voltage results in the reactive component of the tunneling current [21]. Furthermore, the

higher steepness of the nonlinearity of the dc I-V characteristics leads to a larger reactive current component [21]. The two tunneling current components, the reactive and the dissipative, are related through the frequency Kramers-Kronig transformation [21], [22]. The nonlinear susceptance calculated through the Kramers-Kronig transform of the dc I-V curve, could be comparable to the susceptance due to the geometrical junction capacitance and its important contribution was recently demonstrated in [23], [24].

In this paper, the nonlinear susceptance,  $B_{11}$  in [22], was calculated from the measured dc I-V characteristics [21].  $B_{11}$  was calculated for the conditions under which the junction capacitance had been measured: frequency  $f = 4$  GHz, bias voltage  $V_0 = 1$  mV, and the normalized energy of the microwave signal

$$\alpha = \frac{eV_{sig}}{hf} < 5 \quad (1)$$

where  $e$  is the electron charge,  $V_{signal}$  is the voltage amplitude of the microwave signal,  $h$  is the Planck's constant and  $f$  is the measurement frequency. It should be noted that no effects of the RF signal on the IV curves were observed. Depending on the bias voltage, the nonlinear susceptance can be either inductive or capacitive [25]. The calculations showed that in the conditions used for the measurement,  $B_{11}$  is capacitive. Therefore, the nonlinear capacitance ( $C_n$ ) was extracted from the calculated susceptance as

$$C_n = \frac{B_{11}}{2\pi f} \quad (2)$$

The measured junction capacitance ( $C_m$ ), the calculated nonlinear capacitance  $C_n$ , and the corrected capacitance (the true geometrical capacitance), which is

$$C_g = C_m - C_n \quad (3)$$

for the batches with the lowest and the highest  $R_nA$ , 9.4 (since the batch with  $R_nA = 8.8 \Omega \cdot \mu\text{m}^2$  only contained three data points, for the sake of better comparison, batch with  $R_nA = 9.4 \Omega \cdot \mu\text{m}^2$  was demonstrated here) and  $68 \Omega \cdot \mu\text{m}^2$ , are plotted in Figure 3a and Figure 3b, respectively. It is apparent from the figure that the nonlinear capacitance,  $C_n$ , is a substantial contribution for low- $R_nA$  junctions. Interestingly, for the same batch with the same  $R_nA$  (see Figure 3a), the contribution of  $C_n$  is higher for junctions with the smaller  $R_n$ .

### B. $C_s(R_nA)$ relation

The dependence of the measured ( $C_{ms}$ ) and corrected specific capacitance ( $C_{gs}$ ) on the  $R_nA$  value for each batch is illustrated in Figure 4. The error bars on the  $C_{gs}$  data represent the standard error, which were obtained from the linear fit to the capacitance vs. area plots in Figure 2. In a previous study [18], it was shown that the observed scatter in the  $R_nC$  and  $R_nA$  value is a consequence of the tunnel barrier properties, e.g., the tunnel barrier thickness, being non-uniform across the wafer. Given that the employed direct measurement method resulted in high accuracy between  $\pm 2\%$  to  $\pm 11\%$  [18], the observed error bars are therefore another indication that such non-uniformities might give rise to the observed differences in the  $C_s$ .

It can be seen in Figure 4 that  $C_{ms}$  vs.  $R_nA$  data points follow quite tightly the model reported by van der Zant et al. [1]. In

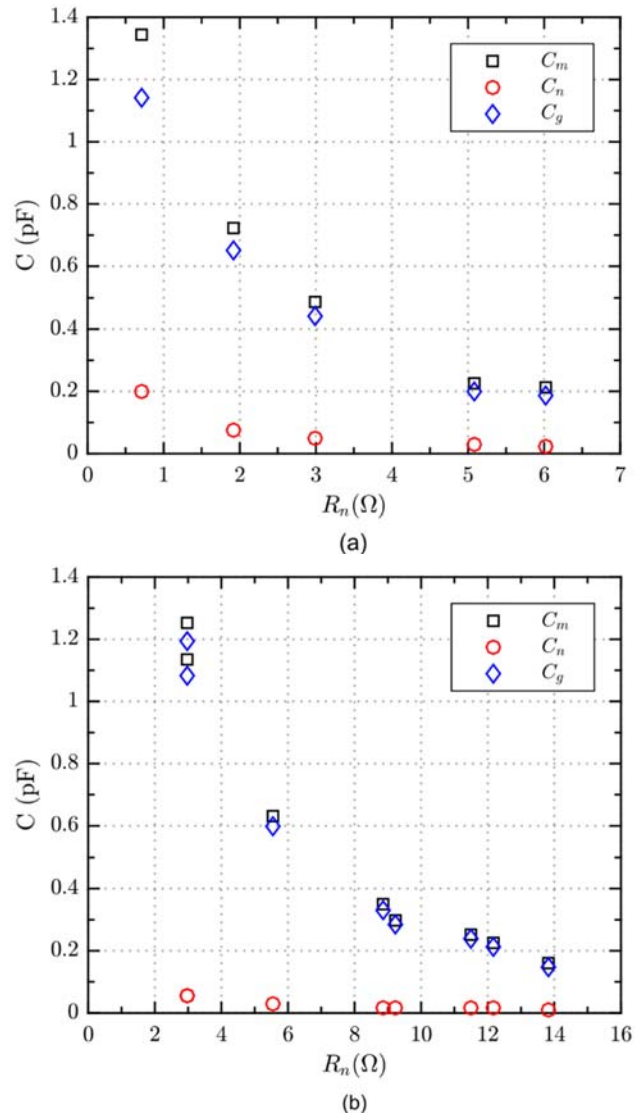


Fig. 3. The nonlinear capacitance  $C_n$  (red circles) is compared with the measured capacitance  $C_m$  (black squares) for two batches with the (a) lowest and the (b) highest  $R_nA$  of 9.4 and  $68 \Omega \cdot \mu\text{m}^2$ , respectively. The blue diamond data points represent the true geometrical capacitance  $C_g$ , which is obtained by the difference of  $C_m$  and  $C_n$  for each  $R_n$ .

that work, the specific capacitance was measured using Fiske mode

resonances in one-dimensional arrays of Josephson junctions. Regarding this type of measurements, in presence of magnetic field and at specific voltages, Fiske resonances appear as enhanced junction current, where the Josephson frequency matches that of the cavity resonance of the junction. Although the Van der Zant et al. model closely follows the  $C_{gs}$  until  $R_nA \approx 20 \Omega \cdot \mu\text{m}^2$ , at lower  $R_nA$  range this model predicts higher values of the specific capacitance than the obtained  $C_{gs}$  in the present work. Given that the nonlinear capacitance is non-negligible at low  $R_nA$  and even at a few GHz input signal frequency, it could be hypothesized that in Fiske type of measurements [9], high frequencies maybe imposed on the SIS junction contributing to the higher measured  $C_s$  values. Hence, Fiske measurements may overestimate the obtained value of the specific capacitance.

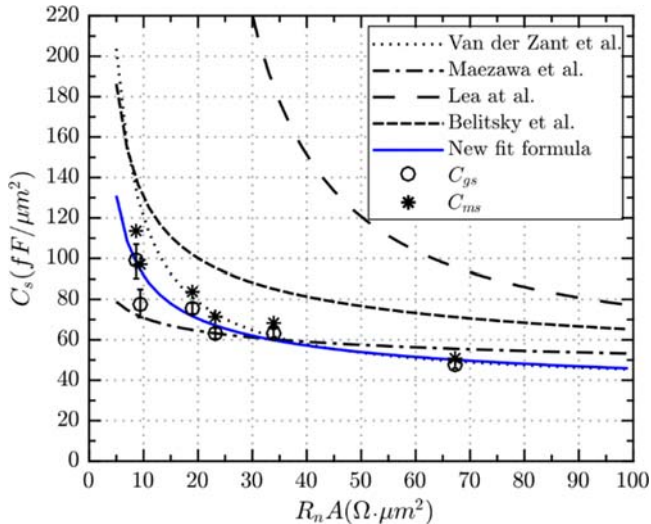


Fig. 4. The measured ( $C_{ms}$ ) and the corrected ( $C_{gs}$ ) specific capacitance presented as asterisk and circle data points, respectively, are compared with the specific capacitance prediction model in [4] and the experimentally obtained relations [1]–[3]. The error bars represent the standard error, which were obtained from the linear fit to the capacitance vs. area plots in Figure 2. The solid blue line is the fit to the  $C_{gs}$  vs.  $R_nA$  using the  $C_s = a/\ln(R_nA)$  formula. This fit resulted in the calibration constant  $a$  equal to 211 instead of 300 from the model [4].

In contrast to what Van der Zant et al. suggests, the model from Maezawa et al. [2] predicts lower values of the  $C_s$  compared with the obtained  $C_{gs}$  at low  $R_nA$  values. In [2], the  $C_s$  was estimated utilizing the resonances in superconducting quantum interference device (SQUID), which were due to the junction capacitance and the loop inductance interaction. The discrepancies between models from Maezawa et al. and Van der Zant et al. and the obtained  $C_{gs}(R_nA)$  could be partly as a result of the local non-uniformities of the tunnel barrier thickness [18]. Such local non-uniformities result in scatter of both the  $C_s$  and the  $R_nA$  values [18]. Since the  $R_nA$  value is defined by the thinnest parts of the tunnel barrier, which is reported to take up about 10% of the junction area [26], for the same  $R_nA$  the tunnel barrier thickness can have different local non-uniformities. At these tunnel barrier thicknesses of the order of 1 nm, the non-uniformities can be very sensitive to the oxide growth conditions and could be unique to each deposition system. Therefore, junctions produced with the same deposition parameters would probably experience different tunnel barrier thickness non-uniformities, which could be another reason contributing to the disagreement between some of the aforementioned  $C_s(R_nA)$  relations. In addition, some specifics of the junction fabrication process, which affect the junction composition or structure such as plasma processing [27], Nb anodization, or thermal aging [19], could also contribute to the observed differences.

Even though the model from Belitsky et al. [4] ( $C_s = a/\ln(R_nA)$  where  $a=300$ , and  $C_s$  and  $R_nA$  are in  $\text{fF}/\mu\text{m}^2$  and in  $\Omega\cdot\mu\text{m}^2$ , respectively) predicts higher  $C_s$  values compared to the obtained  $C_{gs}$ , this model has quite similar trend as the obtained  $C_{gs}(R_nA)$ . Therefore, this model with a different fitting parameter was used to fit to the  $C_{gs}(R_nA)$ . The fitting yielded the new model with  $a = 211$ , which is shown as the solid blue line in Figure 4.

The observed disparity between the reported  $C_s(R_nA)$  models, especially the Lea et al. model, is larger than the observed

scatter of  $C_s$  (note the error bars) possibly from the local non-uniformities of the tunnel barrier. Because of that, we speculate that it was the particular measurement method, which was the main reason for the observed major discrepancy with the other  $C_s(R_nA)$  models. Given that the employed measurement method in this study is direct and has the lowest reported uncertainty, the circuit designers can rely on the obtained  $C_{gs}(R_nA)$  model. For improved accuracy, we suggest employing the direct method for measuring the junction capacitance so that the amount of scatter due to the local non-uniformity of the tunnel barrier thickness can be taken into account for each trilayer deposition system.

In order to verify the validity of the new  $C_s$  value, we used the measured noise temperature of the SHeFI (Swedish Heterodyne Facility Instrument), band 3 (385-500 GHz) DSB mixer (4-8 GHz IF), which has been in operation since 2010 at Atacama Pathfinder Experiment (APEX) telescope. The mixer tuning circuitry was realized by implementing two SIS junctions separated by a section of inductive microstrip line (twin-junction) [28], see Figure 5. The built-in bias-T, which is integrated with the IF transformer circuitry is also depicted in Figure 5.

The DSB noise temperature (averaged over IF band) was obtained by Y-factor measurements performed with a black body placed at the dewar window at the telescope. The DSB noise temperature was modelled by calculating the coupling using the power match and inverting the results into noise temperature with one fitting parameter. Figure 6 illustrates the measured and the modelled DSB noise temperature using the  $C_s$  value from Belitsky et al. [4] and the present work. We note that using the new value of  $C_s = 211/\ln(R_nA)$  offers a greater potential for improvements in mixer performance compared with the previous value by achieving a better performance of the tuning circuitry.

#### IV. CONCLUSION

This paper attempts to give a comprehensive account of possible reasons contributing to the observed disagreement among the reported specific capacitance ( $C_s$ ) vs.  $R_nA$  models and provide a new reliable model. In this regard, the results of the  $C_s$  from 34 tested junctions with various oxygen exposure parameters were considered. Based on the calculation results, it

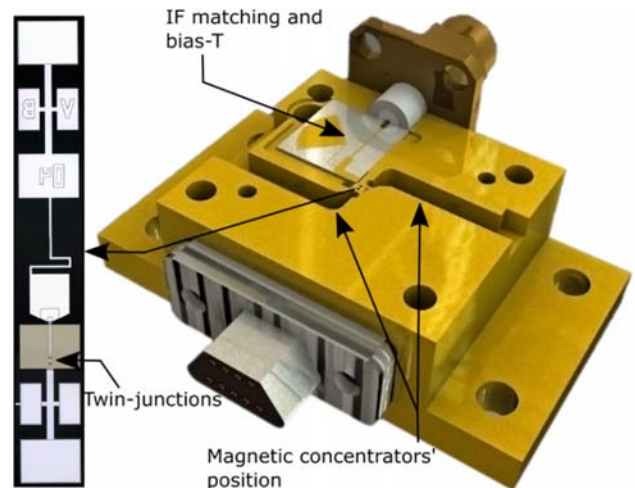


Fig. 5. APEX band 3 mixer block in back-piece configuration. The left-hand side illustration is the zoomed-in mixer chip.

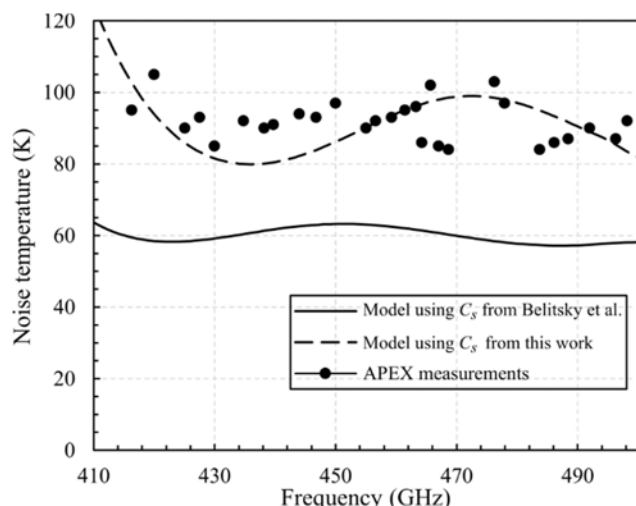


Fig. 6. Comparison of the DSB noise temperature as a function of LO frequency measured at the APEX telescope (solid circles) with the modelled noise temperature using the  $C_s$  value from Belitsky et al. [4] (solid line) and the present work (dashed line).

was shown that the nonlinear susceptance obtained from the Kramers-Kronig transform of the dc I-V curve is comparable to the susceptance resulting from the geometrical junction capacitance particularly for junctions with  $R_n A < 40 \Omega \cdot \mu\text{m}^2$  even at frequencies of a few GHz. It was shown that such non-negligible effects as well as the local non-uniformities of the tunnel barrier thickness might have resulted in the disagreement between some of the existing models and experimentally obtained  $C_s$  ( $R_n A$ ) relations. Using the results of the direct junction capacitance measurement method and accounting for the contributions of the nonlinear capacitance, we propose an improved and more accurate model for the  $C_s$  ( $R_n A$ ) relation using the fitting formula  $C_s = a/\ln(R_n A)$ , where  $a=211$ , and  $C_s$  and  $R_n A$  are in  $\text{fF}/\mu\text{m}^2$  and in  $\Omega \cdot \mu\text{m}^2$ , respectively. The new value of the  $C_s$  was used to model the mixer performance, which was compared with the measured noise temperature of the APEX SHeFI band 3 (385-500 GHz) DSB mixer. The comparison results showed that this  $C_s$  value can greatly improve the performance of SIS mixers.

#### ACKNOWLEDGMENT

The authors would like to acknowledge Sven-Erik Ferm for the machining of the small mechanical parts; Erik Sundin, and Mathias Fredrixon are acknowledged for their help with arrangement of the measurement set up.

#### REFERENCES

- [1] H. S. J. van der Zant, R. a. M. Reuveur, T. P. Orlando, and a. W. Kleinsasser, "One-dimensional parallel Josephson-junction arrays as a tool for diagnostics," *Appl. Phys. Lett.*, vol. 65, no. 16, p. 2102, 1994.
- [2] M. Maezawa, M. Aoyagi, H. Nakagawa, I. Kurosawa, and S. Takada, "Specific capacitance of Nb/AlOx/Nb Josephson junctions with critical current densities in the range of 0.1–18 kA/cm<sup>2</sup>," *Appl. Phys. Lett.*, vol. 66, no. 16, p. 2134, 1995.
- [3] D. M. J. Lea, "Integrated test structures for characterization of thin films for superconductor-insulator-superconductor devices and circuits," Univ. Virginia, 1996.
- [4] V. Belitsky, S. W. Jacobsson, S. A. Kovtonjuk, E. L. Kollberg, and A. B. Ermakov, "100 GHz Mixer with Vertically Integrated (stacked) SIS Junction Array," *Int. J. Infrared Millimeter Waves*, vol. 14, no. 5, pp. 949–957, 1993.
- [5] T. M. Klapwijk, P. Dieleman, and M. W. M. de Graauw, "Pushing the operating range of SIS mixers into the THz regime," *Supercond. Sci. Technol.*, vol. 10, no. 12, pp. 876–879, Dec. 1997.
- [6] C. E. Tong, P. K. Grimes, J. Weintraub, and R. Blundell, "Ultra-wide IF bandwidth -The next frontier for SIS receivers," in *2015 IEEE MTT-S International Microwave Symposium*, 2015, pp. 1–4.
- [7] B.-K. Tan, G. Yassin, and P. Grimes, "Ultra-Wide Intermediate Bandwidth for High-Frequency SIS Mixers," *IEEE Trans. Terahertz Sci. Technol.*, vol. 4, no. 2, pp. 165–170, Mar. 2014.
- [8] C. F. J. Lodewijk, E. Van Zeijl, T. Zijlstra, D. N. Loudkov, F. P. Mena, and A. M. Baryshev, "Bandwidth of Nb / AlN / Nb SIS Mixers Suitable for Frequencies around 700 GHz," no. April, pp. 28–30, 2008.
- [9] A. R. Kerr, "Some fundamental and practical limits on broadband matching to capacitive devices, and the implications for SIS mixer design," *IEEE Trans. Microw. Theory Tech.*, vol. 43, no. 1, pp. 2–13, 1995.
- [10] F. Deppe, "Determination of the capacitance of nm scale Josephson junctions," *J. Appl. Phys.*, vol. 95, no. 5, p. 2607, Feb. 2004.
- [11] G. Sun et al., "Time-resolved measurement of capacitance in a Josephson tunnel junction," *Appl. Phys. Lett.*, vol. 89, no. 8, p. 82516, 2006.
- [12] R. Dolata, H. Scherer, A. B. Zorin, and J. Niemeyer, "Single-charge devices with ultrasmall Nb/AlO[sub x]/Nb trilayer Josephson junctions," *J. Appl. Phys.*, vol. 97, no. 5, p. 54501, Feb. 2005.
- [13] A. B. Pavolotsky, T. Weimann, H. Scherer, J. Niemeyer, A. B. Zorin, and V. A. Krupenin, "Novel method for fabricating deep submicron Nb/AlO/sub x/Nb tunnel junctions based on spin-on glass planarization," *IEEE Trans. Applied Supercond.*, vol. 9, no. 2, pp. 3251–3254, Jun. 1999.
- [14] M. W. Johnson, B. J. Dalrymple, D. J. Durand, and J. A. Luine, "NbN and Nb SFQ device performance," *IEEE Trans. Applied Supercond.*, vol. 13, no. 2, pp. 571–574, Jun. 2003.
- [15] M. Gurvitch, "High quality refractory Josephson tunnel junctions utilizing thin aluminum layers," *Appl. Phys. Lett.*, vol. 42, no. 5, p. 472, Mar. 1983.
- [16] A. W. Lichtenberger, C. P. McClay, R. J. Mattauch, M. J. Feldman, S. Pan, and A. R. Kerr, "Fabrication of Nb/Al-Al/sub 2/O/sub 3/Nb junctions with extremely low leakage currents," *IEEE Trans. Magn.*, vol. 25, no. 2, pp. 1247–1250, Mar. 1989.
- [17] P. Y. Aghdam, H. Rashid, A. Pavolotsky, V. Desmaris, D. Meledin, and V. Belitsky, "Direct Measurement of Superconducting Tunnel Junction Capacitance," *IEEE Trans. Terahertz Sci. Technol.*, vol. 5, no. 3, pp. 464–469, May 2015.
- [18] P. Yadranejee Aghdam, H. Marouf Rashid, A. Pavolotsky, V. Desmaris, and V. Belitsky, "Dependence of the scatter of the electrical properties on local non-uniformities of the tunnel barrier in Nb/Al-AlOx/Nb junctions," *J. Appl. Phys.*, vol. 119, no. 5, p. 54502, Feb. 2016.
- [19] A. B. Pavolotsky, D. Dochev, and V. Belitsky, "Aging- and annealing-induced variations in Nb/Al–AlOx/Nb tunnel junction properties," *J. Appl. Phys.*, vol. 109, no. 2, p. 24502, 2011.
- [20] H. Rashid, D. Meledin, V. Desmaris, A. Pavolotsky, and V. Belitsky, "Superconducting 4–8-GHz Hybrid Assembly for 2SB Cryogenic THz Receivers," *IEEE Trans. Terahertz Sci. Technol.*, vol. 4, no. 2, pp. 193–200, Mar. 2014.
- [21] H. Rashid, V. Desmaris, A. Pavolotsky, and V. Belitsky, "Harmonic and reactive behavior of the quasiparticle tunnel current in SIS junctions," *AIP Adv.*, vol. 6, no. 4, p. 45109, Apr. 2016.
- [22] J. Tucker and M. Feldman, "Quantum detection at millimeter wavelengths," *Rev. Mod. Phys.*, vol. 57, no. 4, pp. 1055–1113, Oct. 1985.
- [23] H. Rashid, S. Krause, D. Meledin, V. Desmaris, A. Pavolotsky, and V. Belitsky, "Frequency Multiplier Based on Distributed Superconducting Tunnel Junctions: Theory, Design, and Characterization," *IEEE Trans. Terahertz Sci. Technol.*, vol. 6, no. 5, pp. 1–13, 2016.
- [24] H. Rashid, V. Desmaris, A. Pavolotsky, and V. Belitsky, "THz Frequency Up-Conversion using Superconducting Tunnel Junction," *IEEE Microw. Wirel. Components Lett.*, vol. 26, no. 10, pp. 831–833, Oct. 2016.
- [25] Q. Hu, C. Mears, P. Richards, and F. Lloyd, "Quantum susceptance and its effects on the high-frequency response of superconducting tunnel junctions," *Phys. Rev. B*, vol. 42, no. 16, pp. 10250–10263, Dec. 1990.

- [26] L. J. Zeng *et al.*, "Direct observation of the thickness distribution of ultra thin AlO<sub>x</sub> barriers in Al/AlO<sub>x</sub>/Al Josephson junctions," *J. Phys. D. Appl. Phys.*, vol. 48, no. 39, p. 395308, Oct. 2015.
- [27] S. K. Tolpygo *et al.*, "Plasma process-induced damage to Josephson tunnel junctions in superconducting integrated circuits," *Supercond. Sci. Technol.*, vol. 20, no. 11, pp. S341–S349, Nov. 2007.
- [28] V. Y. Belitsky and M. A. Tarasov, "SIS junction reactance complete compensation," *IEEE Trans. Magn.*, vol. 27, no. 2, pp. 2638–2641, 1991.